EFDA–JET–PR(11)21

J.P. Graves, I.T. Chapman, S. Coda, M. Lennholm, M. Albergante
and JET EFDA contributors

Control of Magnetohydrodynamic Instabilities by Phase Space Engineering of Energetic Ions in Tokamak Plasmas

Control of Magnetohydrodynamic Instabilities by Phase Space Engineering of Energetic Ions in Tokamak Plasmas

J.P. Graves[1], I.T. Chapman[2], S. Coda[1], M. Lennholm[3], M. Albergante[1]
and JET EFDA contributors*

JET-EFDA, Culham Science Centre, OX14 3DB, Abingdon, UK

[1]École Polytechnique Fédérale de Lausanne (EPFL), Centre de Recherches en Physique des Plasmas, Association EURATOM-Confédération Suisse, 1015 Lausanne, Switzerland
[2]EURATOM-CCFE Fusion Association, Culham Science Centre, OX14 3DB, Abingdon, OXON, UK
[3]EFDA-JET CSU, Culham Science Centre, Abingdon, OX14 3DB, UK
** See annex of F. Romanelli et al, "Overview of JET Results", (23rd IAEA Fusion Energy Conference, Daejon, Republic of Korea (2010)).*

Preprint of Paper to be submitted for publication in
Nature

ABSTRACT

Internally driven magnetohydrodynamic disturbances frequently occur in plasmas when the drive associated with pressure gradients and magnetic geometry exceeds the stabilising magnetic field line bending associated with shear Alfv´en waves. Mirror trapped collisionless energetic ion populations typically interact with such instabilities in the magnetosphere and in toroidal laboratory plasma devices such as the tokamak. Unique to the toroidal configuration are confined energetic particles that are not mirror trapped. Ordinarily in tokamak plasmas, the combined effect of trapped and circulating energetic ions is strongly, but not fully, stabilising to low frequencyMHDoscillations, sometimes resulting in less frequent but dangerously enlarged plasma reorganisation and possible plasma termination. Here, we show that hybrid kinetic-magnetohydrodynamic theory has provided new insight into phase space engineering techniques for controlling stability in the Joint European Torus tokamak. Manipulation of auxiliary ion heating systems can take advantage of the properties of circulating ions, enabling an asymmetry in the distribution of ions in the velocity orientated along magnetic field lines. We show experiments in which large sawtooth collapses have been controlled, and neoclassical tearing modes avoided, in high performance reactor relevant plasmas.

INTRODUCTION

Performance in tokamak plasmas has improved to such an extent that it is expected that the next generation machine, ITER [1], presently under construction, will generate fusion power up to ten times the input power required to maintain its nuclear reactivity. Success in ITER, and in present day tokamaks relies crucially on optimised cross magnetic field particle and energy confinement, as well as control of MagnetoHydroDynamic (MHD) instabilities. Perhaps ironically, the confinement properties of tokamaks have become so good that various techniques are now being deployed to deliberately impair confinement locally in space and sometimes temporally, thereby either avoiding or initiating controlled destabilisation of MHD instabilities. Not doing so can lead to delayed but consequently larger perturbations, which in the case of Edge Localised Modes (ELMS) [2, 3] can damage the vessel wall, and in the case of core localised sawteeth [4], can trigger [5, 6] globally confinement limiting, and potentially disruption causing, Neoclassical Tearing Modes (NTMs) [7].

In tokamaks it is well known that instabilities are primarily driven by steepening gradients in the current density or the pressure. Minority populations of super thermal ions delay the onset of instabilities such as sawteeth (electron temperature traces of Figs. 4 and 5 show typical sawtooth crash cycles), thereby improving confinement properties of tokamaks, allowing steeper pressure and current gradients to develop. World record laboratory fusion power yields were obtained in the Joint European Torus (JET) [8] over a transient period where the core-localised sawtooth instability was avoided. When it was not avoided, neoclassical tearing modes were sometimes [9] triggered at the time of a sawtooth crash event, leading to permanent reductions in fusion power and performance. In the standard physics scenarios of future fusion grade tokamaks such as ITER, it is expected [10] that the large fusion born alpha particle population will strongly lengthen the period between

consecutive sawtooth crash events, but it will probably not be possible to avoid sawteeth altogether [11]. As a consequence, the sawtooth is now accepted as unavoidable, and much recent research has concentrated on finding means of making sawtooth events more frequent, and therefore less likely to trigger secondary instabilities such as NTMs, or to cause disruption. This article reports an innovative means of controlling MHD instabilities, culminating in the application of sawtooth control in high performance fusion reactor relevant scenarios.

1. ENERGETIC ION DYNAMICS IN MAGNETISED PLASMAS

Stabilisation of MHD modes, by virtually collisionless energetic particles, is not unique to tokamak plasmas. Figure 1 compares (a) ion orbits confined in the magnetic field of the earths magnetosphere with (b) ion orbits in the magnetic field lines of the tokamak. The rapid helical cyclotron motion has been averaged out in the tokamak, so that the guiding centres of particles moving in parallel with, and drifting across, the magnetic field lines can be clearly seen. Hence the guiding centre velocity $\boldsymbol{v}_g = \boldsymbol{v}_{||} + \boldsymbol{v}_d$, with the cross magnetic field drift velocity $\boldsymbol{v}_d = (\mathbf{B}/(eB^2)) \times (\mu\nabla B + m_{||}^2\kappa)$ determined by the non-homogeneity in the magnetic field strength B, and the curvature vector of the magnetic field lines κ. Here the magneticmoment $\mu = mv_\perp^2/(2B)$ is an adiabatic invariant over the single particle motion. Magnetically trapped particles occur in both the tokamak and magnetosphere for particles that have sufficientlylarge pitch $\mu\mathcal{E}$, which is conserved over the particle orbit in a static magnetic equilibrium,where $\mathcal{E} = mv_{||}^2 = 2 + \mu B$ is the kinetic energy of the particle. As a magnetically trapped ion follows the magnetic field lines, it will experience varying B, so that the parallel velocity $v_{||} = \sigma\sqrt{2|\mathcal{E} - B|/m}$ will periodically change sign and therefore reverse direction, where $\sigma = \pm 1$. Such magnetically trapped particle orbits are shown in Fig.1 (a) and (b). During the bouncing process along the magnetic field lines, the particle undergoes a cross field drift $\boldsymbol{v}_d$, resulting in an average precession in the toroidal direction ϕ. In a tokamak the toroidal coordinate is an angle of (near) symmetry, as it also is in the magnetosphere assuming a perfect dipole field. The effect of trapped ions, undergoing collisions on a timescale comparable to the bounce frequency, on ballooning (emerging from transverse Alfvén type waves) and kink modes is destabilising. However, the long mean free path kinetic correction associated with collisionless trapped ions is stabilising in both tokamaks [12,13,14] and the magnetosphere [15] providing that the bounce averaged drift precession velocity $\langle \boldsymbol{v}_d \cdot \boldsymbol{e}_\phi \rangle$ is much larger than the toroidal phase velocity $\omega/(nR)$ of the wave, where a perturbation of the type $\sim \exp(-in\phi - i\omega t)$ is assumed, and R is the distance of the field line from the axis of symmetry as indicated in Fig. 1. Particles which do not undergo bounce trapping are lost to the earths atmosphere in Fig. 1 (a). However, in a torus, nonvanishing continuous vector magnetic fields 16 exist, and consequently collisionless particles can in principle follow magnetic field lines indefinitely without being lost. Such circulating ions are known as co or counter passing, with convention defining co passing as those circulating toroidally in the direction of the (Ohmically induced) toroidal current. This article identifies the crucial effects of collisionless co and counter passing particles on general MHD disturbances, including [17, 18] the internal kink mode. The

latter is a core localised pressure and current driven mode, whose stability is intrinsically connected to the sawtooth reconnection event. The novel theoretical advances described here are exploited in the creation of experiments that produce an imbalance in the number, or energy density, of co and counter circulating ions, and in so doing, control the sawtooth instability in high performance tokamak conditions.

2. MECHANISM FOR THE EFFECT OF CIRCULATING IONS ON MHD INSTABILITIES

In order to assess the impact of collisionless energetic ions on stability, the hybrid kinetic MHD model [19, 20] is applicable. The linearised equations follow MHD, except that the closure of the system departs from the equation of state, which is only applicable to collisional populations. Breaking the populations into a core ('c') collisional population and a hot ('h'), essentially collisionless ion population, the linearised equation of motion for components perpendicular to the equilibrium magnetic field $\boldsymbol{B}$ is:

$$\rho \frac{\partial^2 \boldsymbol{\xi}}{\partial t^2} = \delta\mathbf{B} \times \mathbf{B} + \mathbf{J} \times \delta\mathbf{B} - \nabla \delta P_c + \boldsymbol{F}_h \left(\underline{\underline{\delta P_h}}\right) \tag{1}$$

where δ denotes a perturbation, P pressure, J current, ρ is the mass density of the majority collisional ion population, ξ is the fluid displacement, obtained in terms of the perturbed electric field via Ohm's law $dE = i\omega\xi \times B$ (the parallel perturbed electric field is neglected here), and the hot ion perturbed force density

$$\boldsymbol{F}_h = -\nabla \cdot \underline{\underline{\delta P_h}}$$

The tensor δP_h is obtained by taking moments of solution fh of the drift kinetic equation, i.e. the Vlasov equation in reduced phase space. The perturbed distribution function about equilibrium f_h can be written [21] in terms of perturbations of the three quantities that are conserved in the equilibrium state:

$$\delta f_h = -\delta P_\phi \frac{\delta f_h}{\delta P_\phi} - \delta\mu \frac{\delta f_h}{\delta \mu} - \delta\varepsilon \frac{\delta f_h}{\delta \varepsilon} \tag{2}$$

where P_ϕ is the toroidal canonical momentum, which is conserved in toroidally symmetric equilibrium. The dynamics of fast ions outside the remit of collisional processes are essentially contained in the last term of Eq. (2), and in a contribution proportional to E in first term of Eq. (2). In particular, $\delta P_\phi = -(n/\omega)\delta\varepsilon - ZeR\delta A$, with δA_ϕ the perturbed toroidal magnetic vector potential, and $\delta\varepsilon$ is the change of energy observed by the particle due to its drift motion across time varying fields, i.e.

$$\delta W_h = -\frac{1}{2}\int d^3x\, \boldsymbol{\xi}^* \cdot \boldsymbol{F}_h \tag{3}$$

where the electric field is assumed to be gryo averaged, and Ze is the charge of the fast ion. The

dynamics associated with $\delta\mathcal{E}$ describes the effects of kinetic compressibility, and thus naturally replaces the effect of fluid compressibility ordinarily contained in the adiabatic equation of state.

The MHD perturbation takes the form $\xi = \hat{\xi}(r) \exp(im\theta - in\phi - i\omega t)$, where in Fig.2 we choose n = m = 1, which is appropriate for an internal kink mode displacement associated with the sawtooth instability. Shown in Fig. 2 (a) is the radial r component of the normalised internal kink displacement $\hat{\xi}$, or the equivalent poloidal electric field $\hat{\delta}E$ in accordance with Ohm's law, as a function of r. The radial component of the perturbed electric field is also important, but for clarity, its effect is not illustrated in what follows. It is seen that $\hat{\delta}E_\theta$ varies rapidly at the location r_1, which is where the parallel wave vector $(nq - m)/R$ vanishes, i.e. $q(r = r_1) = m/n$, where q measures the pitch along the magnetic field line $d\phi/d\theta$. The poloidal electric field in the $r - \theta$ poloidal plane is also shown in Fig.2 (a), with passing and trapped orbits overlaid. The latter are 200keV ^{3}He ions orbiting in a 3T tokamak magnetic field. Since according to Eq.(3) the quantity $\delta\mathcal{E}$ is a convolution of the drift velocity and the electric field over the guiding centre orbit, the sign (direction) and relative amplitude of the poloidal magnetic drift are also shown. Due to the fact that trapped ions do not complete a full poloidal circuit, the convolution is dominated by a negative poloidal drift (i.e. counter-clockwise in Fig.2 (a)). Integrating over velocity space, and assuming that f_h is a Maxwellian with ^{3}He tail temperature 100keV, parabolically distributed in radius, it is seen in Fig.2 (b) that the radial component of the normalised force $\hat{F}_h$ points inwards. In the context of the momentum equation (1) this states that the reaction of trapped ions to a radially outward displacement $\hat{\xi}_r$ is inwards, i.e. the kinetic trapped ion response attempts to damp the initial perturbation. This effect is responsible for the trapped ion stabilisation of low frequency modes in the magnetosphere [15] and the tokamak [13, 14]. Meanwhile, due to the change of sign in the poloidal electric field over the orbit, the effects of circulating ions on $\delta\mathcal{E}$ are significant only if the ions observe a large variation in δE around the poloidal circuit. This occurs especially for particles confined in the region overlapping a resonant MHD surface, and it is in this respect that the mechanism outlined here is relevant to a broad class of modes including interchange modes [22], toroidal Alfven eigenmodes [23] and resistive wall modes [24]. For the internal kink mode, co-passing ions will observe a larger poloidal electric field in the region where the poloidal drift is positive, and vice-versa for counter-passing ions. This variation in the electric field over the orbit occurs because of the radial drift motion of the single particle across magnetic field lines, as shown in Fig.2 (a). The radial drift excursion Δ_r is enhanced as the energy of the single particle is increased relative to the cyclotron frequency. Moreover, circulating particles that are almost trapped have the largest radial drift excursion, and it is these particles that yield the largest contribution to $\boldsymbol{F}_h$. Plotted in 2 (c) and (d) are the contributions to the radial component of $\boldsymbol{F}_h$ due to the radial excursion of respectively co and counter passing ions. It is seen that for co-passing particles the force points radially inwards close to r_1, and thus acts so as to diminish the initial outward displacement. In contrast, counter passing particles create a force that points radially outward close to r_1. In this sense, the counter passing ions have the opposite dynamics to energetic trapped ions, and attempt to amplify the initial outward radial fluid displacement. We

note that the forces plotted in Fig.2 have the same normalisation, and hence it is seen that passing ion kinetic effects compete with trapped ion kinetic effects. Simulations undertaken with effective tail temperature larger than 100keV for the same cyclotron frequency, show [26] that passing ion kinetic effects are dominant by virtue of the enhanced radial guiding centre motion.

3. TOKAMAK EXPERIMENTS EXPLOITING PHASE SPACE ASYMMETRY TO CONTROL SAWTOOTH INSTABILITY

The effects of co and counter passing ions shown in Fig.2 (c) and (d) almost cancel if the distribution of fast ions is symmetric in the parallel velocity $v_{\|}$. If f_h is symmetric in $v_{\|}$ there is a typically small Landau resonance effect that can account for fishbone activity [25]. In Fig.3 we quantify the degree of asymmetry for auxiliary heating methods used in sawtooth control experiments in JET. We apply this approach to low auxiliary power JET Pulse No: 76189, which was designed [26] to verify the fast ion control mechanism [18] illustrated in Fig. 2. The application of low power co-current Neutral Beam Injection (NBI) increases [17, 27] the sawtooth period. An illustration of the co-current NBI is shown in Fig.3(a), while Fig.3(b) plots the radial deposition of the current associated with the fast ions. The current is essentially the parallel velocity moment of f_h, and is therefore a measure of the degree of parallel velocity asymmetry through the plasma. By choosing a radial location close to the resonant surface r_1, and a poloidal angle $\theta = 0$, we plot in Fig.3(c) a simulation [28] of the distribution f_h of fast ions driven by NBI as a function of the parallel and perpendicular velocity. As expected for mirror trapped particles, the distribution is close to symmetric in the trapped cone, while there is a significant asymmetry in the distribution of co and counter passing particles. The co passing particles and the trapped particles stabilise the internal kink mode, and therefore sawteeth, by virtue of the mechanism visualised respectively in Figs.2 (c) and 2 (b). In JET Pulse No: 76189, sawteeth were subsequently controlled, or shortened by depositing ^{3}He minority Ion Cyclotron Resonance Heating (ICRH) close to the resonant surface r1, as seen in simulation [29] shown in Fig. 3(d). The heating location on the high field side of the device at 2.78m, corresponding to a 33MHz Ion Cyclotron Resonance Frequency (ICRF) wave with toroidal field of 2.9T, is shown. Counter current propagating waves were employed (-90^o phasing) in order to preferentially heat counter passing ions. The reason for the extremely effective control on sawteeth is indicated by inspecting the ICRH driven current density in Fig.3(e), where it is seen that the simulations [29] yield very localised asymmetries in the parallel velocity. Figure 3(f) plots the distribution function of ICRH ^{3}He ions close to the resonant surface r_1, where it is seen that a large tail is generated for negative (counter Ohmic current) parallel velocity. In Ref. [26] it was explained that the fast ion mechanism illustrated in Fig.2 could be verified and isolated as the explanation for measured sawtooth control, by a series of JET pulses which successfully varied the asymmetry observed in Fig.3(f), with little effect on the auxiliary coupled power, nor on the net current and pressure profiles (usual collisional MHD instability drives). In essence, the experiments varied the length of the parallel velocity tail observed in Fig. 3(f), and in so doing, the radial and poloidal drift velocities and excursions were varied, and consequently also the reaction force exhibited in

Fig.2(d). This has been verified [26] in detail with evaluation of the fast ion contribution to the internal kink growth rate, and by experimental comparison with sawtooth characteristics.

It is crucial that sawtooth control is demonstrated in reactor relevant high performance conditions. Consequently the experiments addressed by this paper make the leap to conditions akin to those in ITER, the design of which has been made possible because of our growing understanding of fast ion interaction with sawteeth, as reviewed in Refs. [30, 31]. These JET experiments have been designed with large auxiliary heating power, where enhanced NBI power takes the place of fusion alpha particles in ITER. Sawteeth are controlled by toroidally propagating ICRF waves, with low concentration minority 3He, as envisaged for the ICRH design in ITER. The concentration of the minority species is about 1 percent, which has been shown experimentally and with simulations [26], to be the optimum compromise between requiring high energy minority tail temperature to enlarge the drift orbit excursions, and enabling efficient power transfer between ICRF wave and minority population. High auxiliary power is sought, but otherwise the configuration is the same as the earlier JET Pulse No: 76189 [26] shown in Fig.3. As is seen in Fig.4 by inspection of JET pulse 78768, 4.8MW of neutral beams stabilises the sawteeth by lengthening their period from around 70ms to 500ms. Following this, the application of -90^{o} phased ICRH at 5MW reduces the sawtooth period to around 200ms despite the increase in energy confinement time (see the stored energy (W_{dia}) in Fig.4) and resistive diffusion time due to the increased stored energy and conductivity. Also shown in Fig. 4 is the amplitude of the n = 1 magnetic field perturbation, driven deliberately large by the application of ICRH, which successfully destabilises the internal kink mode via the large population of energetic counter-passing ions. In an otherwise similar pulse also shown in Fig.4, JET Pulse No: 78773 begins with an enhanced NBI power of 6.4MW, which once again creates 500ms sawteeth. The application of 5MW of ICRH is sufficient to enhance the auxiliary power above the level required to create a high confinement mode, or H-mode. In this mode of operation, large pressure gradients are created at the plasma edge, which in turn create edge localised modes, seen by the H_{α} signal in Fig.4, but have the benefit of raising the density and temperature in the core, as evidenced by the enhancement in the stored energy increasing W_{dia}. These ITER relevant 3He minority ICRH experiments demonstrate for the first time that sawteeth in H-mode can be efficiently controlled by phase space engineering, where the sawtooth period has been reduced by a factor of two in this case.

Let us now examine ITER relevant standard scenario conditions without proactive sawtooth control in order to demonstrate the need for it. By reversing the antenna phasing (to $+90^{o}$) relative to Pulse No's: 78768 and 78772 shown in Fig. 4, co-current propagating waves in Pulse No: 78773 enhance the tail of co-passing ions, which in turn stabilise sawteeth. In this respect the combined NBI and ICRH simulate the sawtooth stabilising role of fusion alpha particles. In Fig.5(a) it is seen that following the application of ICRH the longest sawtooth period exceeds one second, which is more than an order of magnitude longer than during the Ohmic phase of the pulse. Despite being in low confinement mode (in contrast to JET Pulse No: 78773 in Fig.4), the magnetics signal indicates the growth of an n = 2 mode directly following the crash of the long sawtooth. The amplitude of this NTM

is large enough to reduce the stored energy, and moreover, towards the end of the pulse, the auxiliary power, current, magnetic field and density are ramped down automatically as a precaution against plasma disruption. Figure 5(b) shows a magnetics spectrogram during the ICRH phase of pulse 78773. It is seen that various modes are triggered following each consecutive sawtooth crash, but each of these secondary modes disappears except the n = 2 NTM following the fast ion driven long sawtooth.

The simulations shown in Fig. 6 predict that the stabilising effect of fusion alpha particles on ITER sawteeth could be completely neutralised with 20MW of low concentration (1 percent) ^{3}He minority ICRH in a standard deuterium-tritium ITER plasma scenario 1. The fast ion mechanism described, and experimentally demonstrated, in this article, is quantified in Fig.6 in terms of the potential energy integrated over the plasma volume

$$\delta W_h = -\frac{1}{2}\int d^3x\, \boldsymbol{\xi}^* \cdot \boldsymbol{F}_h$$

where ξ^* is the complex conjugate of ξ. The potential energy is obtained in terms of the perturbed force $\boldsymbol{F}_h$ for each each fast ion species, as calculated in Fig.6. The total fast ion energy is the sum of these terms. These simulations, obtained from the HAGIS [30, 32] guiding centre code, demonstrate that while both the fast ion population generated from the 1MeV ITER co-current NBI system design at 33MW, and the simulated fusion alpha particle population, are stabilising (positive δW) to an internal kink mode displacement in ITER, the ICRH population is strongly destabilising (negative δW) providing the ICRH resonance radius rres is sufficiently close to the internal kink mode resonant surface r_1. These ITER dedicated simulations, together with the JET experiments reported here, greatly increase confidence that NTMs and disruptions triggered by sawteeth can be avoided in ITER. Furthermore, additional control techniques [30, 31], such as electron cyclotron current drive, will be much more effective in plasmas where ICRH has nullified the stabilising effects of alpha particles.

CONCLUSIONS

A mechanism has been identified capable of controlling MHD instabilities by velocity phase space engineering in tokamaks. The mechanism is unique to a toroidally confined plasma, in which energetic particles that are not magnetically bounce trapped can be distributed asymmetrically in the velocity parallel to the magnetic field. Such a population can damp or enhance the growth rates of MHD oscillations ordinarily driven internally by gradients in the plasma pressure. The experiments described here deliberately create such an energetic ion population in order to successfully control crucial core localised sawteeth and neo-classical tearing modes in (ITER) fusion reactor relevant high performance tokamak plasmas.

ACKNOWLEDGEMENTS

The authors of are grateful to B. Alper, M. de Baar, K. Crombe, L.-G. Eriksson, R. Felton, D. Howell, V. Kiptily, H.R. Koslowski, M.-L. Mayoral, I. Monakhov, I. Nunes, S. D. Pinches and JET-EFDA

contributors for assistance with JET experiments. Simulations undertaken by M. Jucker, T. Johnson and O. Asunta are also gratefully acknowledged. This work, supported by the Swiss National Science Foundation, and by the European Communities under contract of Association between EURATOM and Confédération Suisse, was carried out within the framework of the European Fusion Development Agreement. The views and opinions expressed herein do not necessarily reflect those of the European Commission. Author Contributions J.P.G. conceived and wrote the manuscript, led the theory and jointly devised and led the experiments with I.T.C., S.C and M.L. Numerical simulations were performed by M.A., I.T.C and J.P.G. Additional Information The authors declare that they have no competing financial interests

REFERENCES

[1]. ITER Physics Basis, Nuclear Fusion **47** S1 (2007)

[2]. T.E. Evans, R.A. Moyer, K.H. Burrell, M.E. Fenstermacher, I. Joseph, A.W. Leonard, T.H. Osborne, G.D. Porter, M.J. Schaffer, P.B. Snyder, P.R. Thomas, J.G.Watkins and W. P. West, Nature Phys. **2** 419 (2006)

[3]. Y. Liang, H.R. Koslowski, P.R. Thomas, E. Nardon, B. Alper, P. Andrew, Y. Andrew, G. Arnoux, Y. Baranov, M. Bcoulet, M. Beurskens, T. Biewer, M. Bigi, K. Crombe, E. De La Luna, P. de Vries, W. Fundamenski, S. Gerasimov, C. Giroud, M. P. Gryaznevich, N. Hawkes, S. Hotchin, D. Howell, S. Jachmich, V. Kiptily, L. Moreira, V. Parail, S.D. Pinches, E. Rachlew, and O. Zimmermann, Physical Review Letters **98**, 265004 (2007)

[4]. S. von Goeler, W. Stodiek and N. Sauthoff, Physical Review Letters **33**, 1201 (1974)

[5]. D.J. Campbell, D.F.H. Start, J.A. Wesson, D.V. Bartlett, V.P. Bhatnagar, M. Bures, J.G. Cordey, G.A. Cottrell, P.A. Dupperex, A.W. Edwards, C.D. Challis, C. Gormezano, C.W. Gowers, R.S. Granetz, J.H. Hammen, T. Hellsten, J. Jacquinot, E. Lazzaro, P.J. Lomas, N. Lopes Cardozo, P. Mantica, J. A. Snipes, D. Stork, P.E. Stott, P. R. Thomas, E. Thompson, K. Thomsen, and G. Tonetti, Physical Review Letters **60**, 2148 (1988)

[6]. O. Sauter, E. Westerhof, M.L. Mayoral,4, B. Alper, P. A. Belo, R.J. Buttery, A. Gondhalekar, T. Hellsten, T.C. Hender, D.F. Howell, T. Johnson, P. Lamalle, M.J. Mantsinen, F. Milani, M.F. F. Nave, F. Nguyen, A.L. Pecquet, S.D. Pinches, S. Podda, and J. Rapp, Physical Review Letters **88**, 105001 (2002)

[7]. R.B. White, D.A. Monticello, M.N. Rosenbluth and B.V. Waddel, Physics of Fluids **20**, 800 (1977)

[8]. J. Jacquinot and the JET Team, Plasma Physics and Controlled Fusion **41**, A13 (1999).

[9]. M.F.F. Nave, N.N. Gorelenkov, K.G. McClements, S.J. Allfrey, B. Balet, D.N. Borba, P.J. Lomas, J. Manickam, T.T.C. Jones, P.R. Thomas, Nuclear Fusion **42** 281, (2002)

[10]. F. Porcelli, D. Boucher and M. N. Rosenbluth, Plasma Physics and Controlled Fusion **38**, 2163 (1996).

[11]. I.T. Chapman, R.J. Buttery, S. Coda, S. Gerhardt, J.P. Graves, D.F. Howell, A. Isayama, R.J. La Haye, Y. Liu, P. Maget, M. Maraschek, S. Sabbagh, O. Sauter, the ASDEX Upgrade, DIIID, HL-2A, JT-60U, MAST, NSTX, TCV and Tore Supra Teams and JET-EFDA Contributors Nuclear Fusion **50** 102001 (2010)

[12]. F. Porcelli, M. N. Rosenbluth, Plasma Physics and Conrolled Fusion **40**, 481 (1998)

[13]. R.B. White, P. H. Rutherford, P. Colestock, and M. N. Bussac, Physical Review Letters **60**, 2038 (1988)

[14]. F. Porcelli, Plasma Physics and Conrolled Fusion **33**, 1601 (1991).
[15]. C.Z. Cheng and Q. Qian, Journal of Geophysical Research **99**, 11193 (1994)
[16]. L.E.J. Brouwer, "On continuous vector distributions on surfaces", Nederl. Akad. Wetensch. Proc. Ser. A **11**, 850858 (1909)
[17]. J.P. Graves, Physical Review Letters **92** 185003 (2004)
[18]. J.P. Graves, I. T. Chapman S. Coda, L. -G. Eriksson and T. Johnson, Physical Review Letters 102 065005 (2009)
[19]. T. M. Antonsen, Jr., and Y. C. Lee, Physics of Fluids **25**, 132 (1982)
[20]. J. W. Van Dam, M. N. Rosenbluth and Y. C. Lee, Physics of Fluids **25,** 1349 (1982)
[21]. P. Helander, C.G. Gimblett, R.J. Hastie and K.G. McClements, Physics of Plasmas **4**, 2181 (1997)
[22]. C. Mercier, Nuclear Fusion **1**, 47 (1960)
[23]. C.Z. Cheng, Lui Chen and M. S. Chance, Annals of Physics **161**, 21 (1985)
[24]. A. Bondeson and D. Ward, Physical Review Letter **72**, 2709 (1994)
[25]. R. Betti and J. P. Freidberg, Physical Review Letter **70**, 3428 (1993).
[26]. J.P. Graves, I.T. Chapman, S. Coda, T. Johnson, M. Lennholm, B. Alper, M. de Baar, K. Crombe, L.-G. Eriksson, R. Felton, D. Howell, V. Kiptily, H.R. Koslowski, M.-L. Mayoral, I. Monakhov, I. Nunes and S.D. Pinches and JET-EFDA Contributorsa, Nuclear Fusion **50**, 052002 (2010)
[27]. I.T. Chapman, I. Jenkins, R.V. Budny, J.P. Graves, S. D. Pinches and S. Saarelma, Plasma Physics and Conrolled Fusion **50**, 045006 (2008)
[28]. M. Albergante, J.P. Graves, A. Fasoli, M. Jucker, X. Lapillonne and W.A. Cooper, Plasma Physics and Conrolled Fusion **53**, 054002 (2011)
[29]. M. Jucker,, J.P. Graves, W.A. Cooper, N. Mellet, T. Johnson and S. Brunner, Computer Physics Communication. **182**, 912 (2011)
[30]. I. T. Chapman Plasma Physics and Conrolled Fusion **53** 003001 (2011)
[31]. J. P. Graves, I. T. Chapman, S. Coda, T. Johnson, M. Lennholm, J. I. Paley, O. Sauter, Fusion Science Technolgy **59** 539 (2011)
[32]. S. D. Pinches, L. Appel, J. Candy, T. Hender, K. I. Hopcraft, Computer Physics Communication. **111**, 133 (1998)

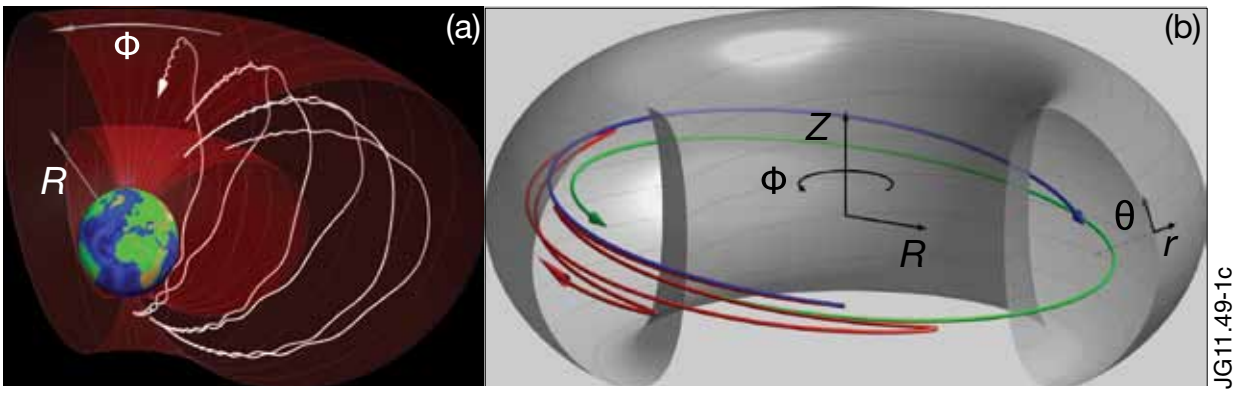

Figure 1: Showing energetic ion orbits confined to the magnetic equilibrium field (field lines shown in grey) of (a) earths magnetosphere and (b) the tokamak. Three essential types of orbits are possible in a configuration where field lines lie on a toroidal surface: trapped (red), co-passing (blue), and counter-passing (green). Also shown is the toroidal angle ϕ, along which the dipole and toroidal systems are symmetric, the major radius R, vertical coordinate Z, poloidal coordinate θ and minor radius coordinate r in a torus.

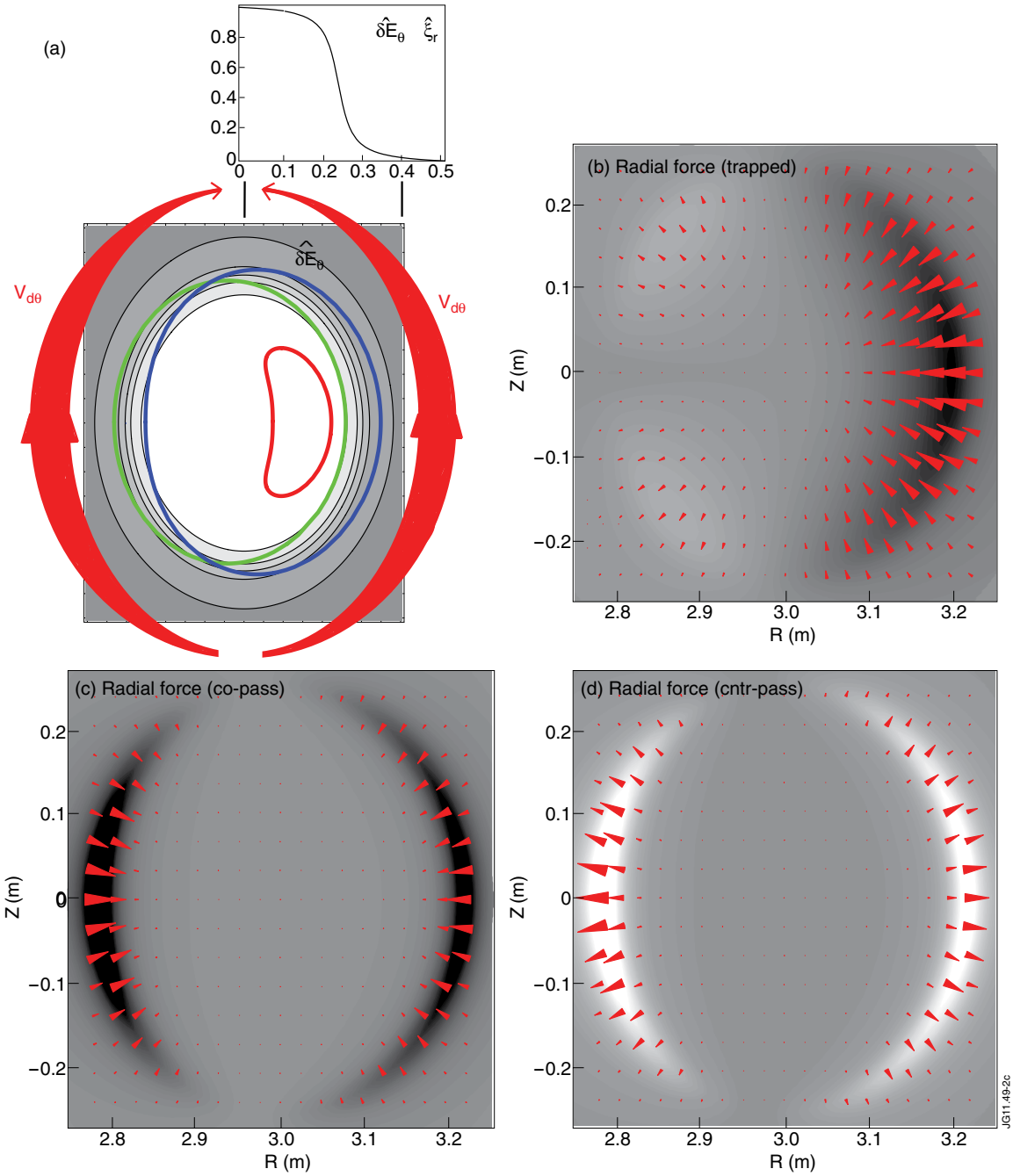

Figure 2: Showing (a) the radial profile of the normalised poloidal electric field $\hat{\delta E}_\theta$, or equivalently the normalised radial fluid displacement $\hat{\xi}_r$, for an internal kink displacement. Also, a contour plot of the poloidal electric field $\hat{\delta E}_\theta$ across the poloidal cross section is shown in (a) in conjunction with trapped (red), co passing (green) and counter passing (blue) ^{3}He ion orbits each with energy 200keV in toroidal field 3T, together with an illustration of the direction and amplitude of the poloidal drift velocity $v_{d\theta}$. (b) plots the radial component of the trapped ion contribution to the response force F_h, while (c) and (d) plot the corresponding contributions due to the radial excursion of respectively co and counter passing ions. The assumed 3He Maxwellian ion population is distributed parabolically in radius.

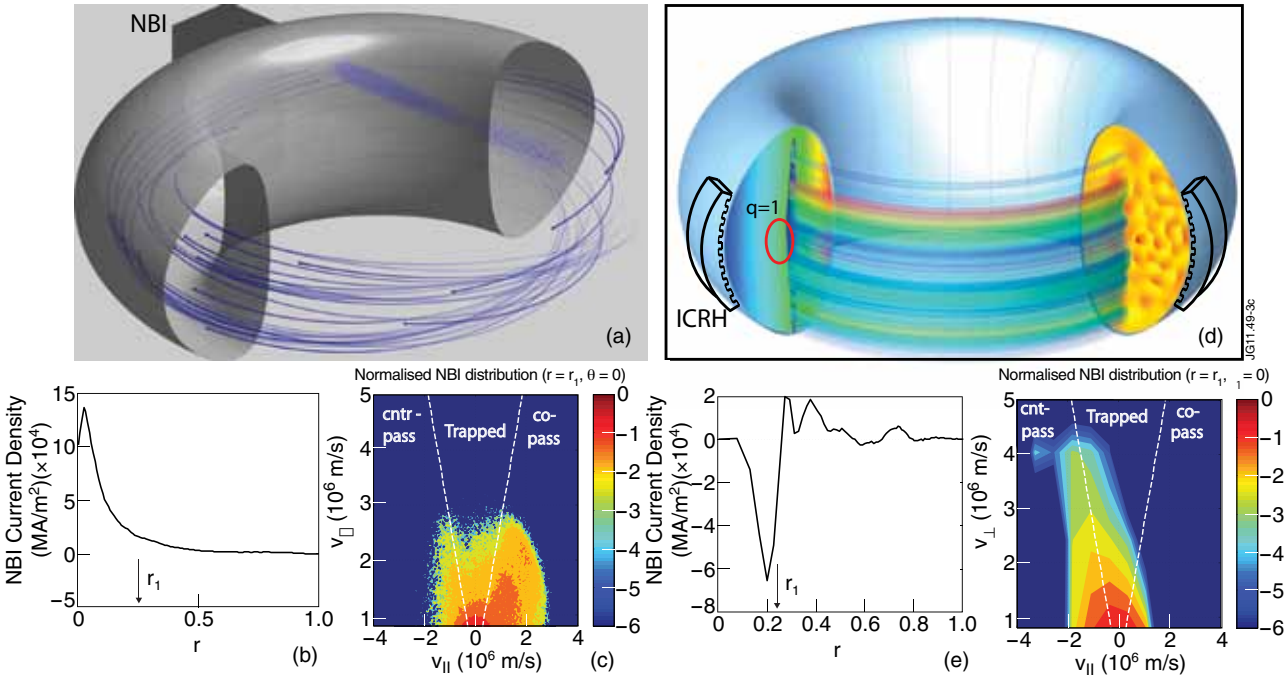

Figure 3: Showing (a) the NBI system orientation, particle ionisation 'cloud', and ion orbit over 5μs following NBI switch on. Showing in (b) the NBI driven current profile in JET Pulse No: 76189 [26], and in (c) the distribution of NBI deuterium ions on the low field side close to the rational surface r_1 (colour-map on logarithmic scale). Shown in (d) is a sketch of two of the four toroidally spaced A2 ICRH antennas in JET, together with the simulated 29 effects of ICRH: the poloidal cut on the left shows the magnetic field strength, line of ICRH resonance and the q = 1 surface. Shown on the right cut is the E- electric field driven by ICRH, while in three dimensions the power deposition is shown through the line of ICRH resonance. In (e) the ICRH driven current profile is shown for JET Pulse No: 78769, and in (f) the distribution of ICRH ions at the same location, and colour-map scaling as the NBI distribution in (c).

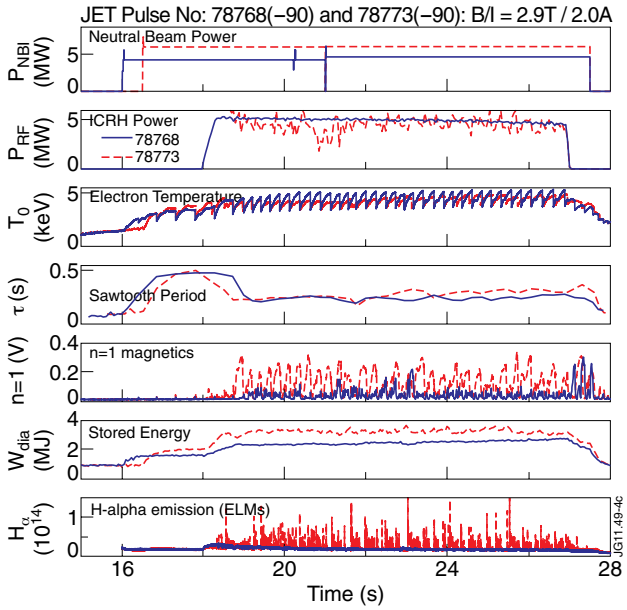

Figure 4: Showing JET Pulse No: 78768 (in blue) with 4.8MW of NBI, and JET Pulse No: 78773 (in red) with 6.4MW of NBI, where both employed low concentration He3 minority ICRH at around 5MW. In both, the −90° antenna phasing produces counter current propagating waves which shorten the sawtooth period, shown by τ (s). Also shown is the central electron temperatures in the core, the stored energy W_{dia}, the n = 1 magnetic perturbation amplitude, and H_α emission, which indicates that Pulse No: 78773 is in high confinement H-mode.

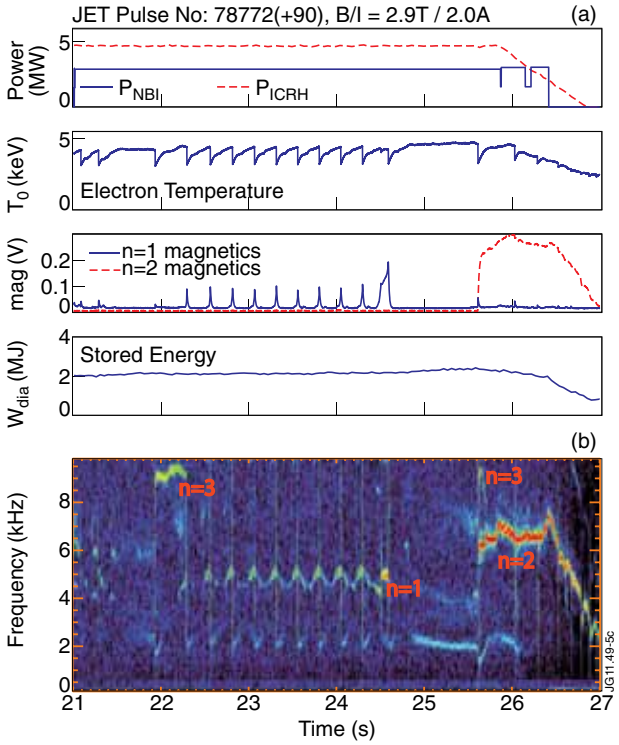

Figure 5: Showing JET Pulse No: 78772 in which low concentration He3 minority ICRH at around 5MW is deployed with +90^o antenna phasing. This produces co-current propagating waves, thus creating a large tail in the co-passing ion phase space, and long sawteeth. A long sawtooth period triggers a n/m = 3/2 NTM despite the pulse being in low confinement mode. In (a) the time traces show the auxiliary power, the central electron temperature, the stored energy and the n = 1 and n = 2 magnetics fluctuation amplitude. Shown in (b) is a magnetics spectrogram during the ICRH phase of Pulse No: 78772, indicating the modes triggered by each consecutive sawtooth crash.

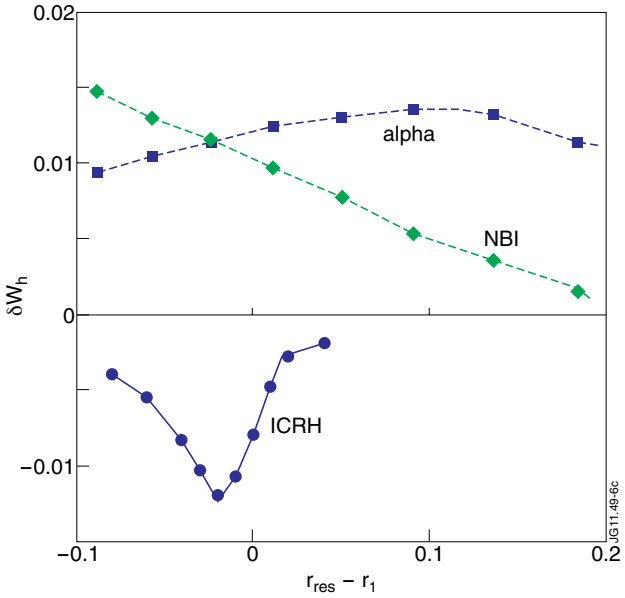

Figure 6: Simulations of the δW contributions to the internal kink mode from alpha particles, neutral beam ions (33MW) and ICRH ions (20MW), assuming one percent ^{3}He minority in a standard deuterium-tritium ITER plasma scenario 1. These are plotted against the difference between ICRH resonance position r_{res} and the internal kink mode resonance radius r_1. In the simulations r_{res} was held constant on the low field side of the device, and r_1 varied.